DOI: 10.1002/ejic.201100051

Molecular Assemblies Based on Polytungstate Clusters and the Flexible Organic Ligand 1,3-Bis(4-pyridyl)propane

Zhangang Han,*[a] Yanna Wang,[a] Xuejun Song,[b] Xueliang Zhai,[a] and Changwen Hu*[c]

Keywords: Polyoxometalates / Copper / Ligand flexibility / Anions / Supramolecular chemistry

Four polyoxometalate (POM) assemblies based on the flexible organic ligand 1,3-bis(4-pyridyl)propane (bpp) have been synthesized and fully characterized, including $(Hbpp)_3[PW_{12}O_{40}]$ (**1**), $[Cu(bpp)]_2[Cu_2(bpp)_3][SiW_{12}O_{40}]$ (**2**), $[Cu_2(Hbpp)_4](H_2bpp)_{0.5}H_2[SbW_{18}O_{60}]\cdot 3H_2O$ (**3**), and $(H_2bpp)_5[Ni_4(OH_2)_2(AsW_9O_{34})_2]\cdot 0.5H_2O$ (**4**). Compounds **1** and **2** were prepared by the reaction of the classical Keggin-type anions with organic bpp under hydrothermal conditions. The difference between these compounds is that protonated bpp is found in **1**, whereas in **2** Cu^I-bpp fragments are present. In the framework of **1**, organic and hybrid chains, built upon supramolecular interactions, coexist. Compound **2**, which crystallizes in a chiral space group, has a 2D wave-like structure consisting of $\{Cu_6(bpp)_6\}$ grids that accommodate $\{[Cu_2(bpp)_2][SiW_{12}O_{40}]\}^{2-}$ fragments. The nonclassical anionic clusters in **3** and **4** are obtained from simple inorganic salts or oxides under hydrothermal conditions. The inorganic moiety in **3** exhibits a pseudo-Dawson-like $[SbW_{18}O_{60}]^{9-}$ cluster, and in **4** a sandwich-type $[Ni_4(H_2O)_2(AsW_9O_{34})_2]^{10-}$ anion is present. The organic ligand bpp, with a freely rotatable $-(CH_2)_3-$ group, is present in various conformations in the four compounds. Structure-analyses results indicate that the flexibility of bpp plays a significant role in the fabrication of these kinds of inorganic-organic arrangements. The thermal and electrochemistry properties of all four compounds have also been studied.

Introduction

Polyoxometalate (POM) clusters that have unrivalled structural diversity offer interesting and exciting perspectives for the design of hybrid materials for application in fields such as catalysis, nonlinear optics, and medicine.[1,2] As they are sub-nanoscale to protein-sized anions, POMs have been employed as important inorganic building blocks for constructing novel hybrid materials containing various organic molecules.[3–5] Such assemblies not only combine the advantages of inorganic oxo–metal clusters and organic molecules through structural fine-tuning, but they also benefit from the close interaction and synergistic effect among the inorganic and organic moieties.[6,7] A current focus in this field is to explore novel lattice architectures that result from the association of organic molecules and POM anions. Therefore, POM chemistry has become one of many areas in inorganic chemistry that is developing rapidly.[8–10]

The high number of oxygen atoms located on the spherical surface of POMs endows them with plenty of opportunities to participate in hydrogen-bonding interactions with organic moieties. Therefore, these polyanions may direct the ordered assembly of organic moieties through the creation of directional hydrogen bonds such as N–H···O and C–H···O, etc. Our research has focused on the synthesis of POM-based assemblies by utilizing the weak interactions that occur between the surface oxygen atoms of the POMs and organic molecules.[11,12] In our ongoing efforts to develop synthetic and functional analogues of POM-based hybrids, we have reported a new family of supramolecular architectures based on POM anions and decorated bipyridine cations that have rigid and conjugated structures such as 2,4′-bipyridine (bpy), 4-(5-chloropyridin-2-yl)pyridine (cpy), 4-(5-phenylpyridin-2-yl)pyridine (ppy), and 4-[5-(4-bromophenyl)pyridin-2-yl]pyridine (bppy).[13] These results illustrate that POM anions can direct these kinds of rigid and conjugated organic molecules into parallel and ordered arrangements. To further investigate the relationship between network connectivity and the types of anions and cations used in the network preparation, in the current work the ability of the flexible organic ligand bpp, which contains a $-(CH_2)_3-$ unit, to assemble POM clusters is explored. Four compounds, **1**–**4**, have been prepared and

[a] College of Chemistry & Material Science, Hebei Normal University,
Shijiazhuang, Hebei 050016, China
Fax: +86-311-8626-9217
E-mail: hanzg116@yahoo.com.cn
[b] College of Physics Science and Information Engineering, Hebei Normal University,
Shijiazhuang, Hebei 050016, China
[c] Institute for Chemical Physics, Department of Chemistry, Beijing Institute of Technology,
Beijing 100081, China
E-mail: cwhu@bit.edu.cn

Supporting information for this article is available on the WWW under http://dx.doi.org/10.1002/ejic.201100051.

characterized. The structural features of these compounds have been investigated, and reveal that the inorganic anions and the structural flexibility of bpp play important roles in the self-organization processes involved in the formation of these assemblies.

Results and Discussion

Synthesis and Structures

The crystal structure analyses of **1**–**4** revealed that all four compounds are formed from organic bpp and different polytungstate clusters: α-Keggin clusters are observed in **1** and **2**, a pseudo-Dawson cluster in **3**, and a sandwich-type heteropolyoxoanion is present in **4** (Figure 1). Compared with rigid conjugated organic molecules (bpy, ppy, cpy and bppy), bpp possesses two pyridine rings linked by $-(CH_2)_3-$ groups, which endows it with a more flexible geometry that influences the assembly of the POM clusters in the solid state. Bridging bpp ligands are usually regarded as excellent candidates for the construction of hybrid solids with high dimensionality due to their flexibility that results in them having a large number of conformational degrees of freedom (TT, TG, GG′, GG).[14]

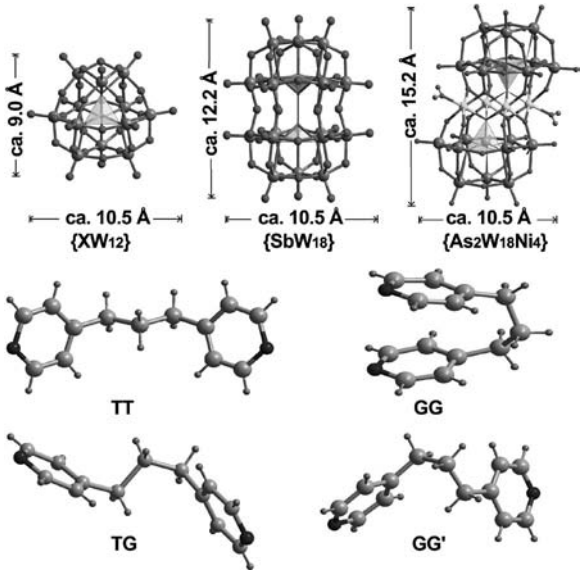

Figure 1. Illustrations showing the sizes and the structures of inorganic anions and the different conformations of the organic ligand bpp in **1**–**4**.

Under routine preparation conditions the integrated Keggin- and Dawson-type POMs are usually used as raw materials for the synthesis of POM-based hybrid materials in which the structures of the anionic clusters are maintained completely. Compounds **1** and **2** were obtained from classical Keggin anions and organic bpp under hydrothermal conditions. The saturated anions are retained in their original forms, i.e. without structural collapse in compounds **1** and **2**. Compound **1** exhibits a supramolecular assembly containing a network of organic and hybrid chains. Compound **2** is representative of a chiral 2D wave-like coordinated polymer that includes the secondary metal group (SMG) Cu–bpp. The nonclassical anionic clusters in compounds **3** and **4** are obtained from simple inorganic salts or oxides. The inorganic moiety in **3** exhibits a pseudo-Dawson-like $[SbW_{18}O_{60}]^{9-}$ cluster, and in **4** a sandwich-type $[Ni_4(H_2O)_2(AsW_9O_{34})_2]^{10-}$ structure is present. The incorporation of different types of anions in **1**–**4** was achieved by the careful adjustment of synthetic reaction conditions. The mechanism for the formation of the different assemblies is not yet understood. However, it appears that the appropriate combination of starting materials, the sizes and ratio of the anions and cations, reaction solution acidity, and hydrothermal synthetic conditions can lead to the formation of POM-based supramolecular structures with different geometrical and structural characteristics (Scheme 1).

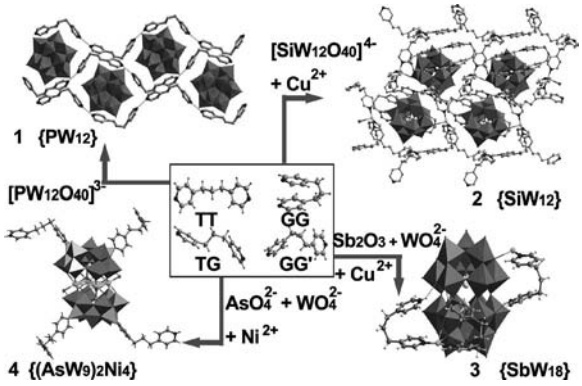

Scheme 1. Reactants for the preparation of **1**–**4** and final products from these corresponding reactions.

The Cu^{II} ions, which have a d^9 electronic configuration and are present in the reaction solutions, are converted to Cu^{I} ions prior to incorporation in the products **2** and **3**, which are prepared under hydrothermal conditions and in the presence of different types of reducers.[15] Bond valence sum calculations[16] for compounds **1**–**4** show that all W ions are in the +6 oxidation state, the Cu ions are in the +1 oxidation state (Table S1, Supporting Information), the Ni atoms are in the +2 oxidation state, the Sb ions are in +3 state, the P and As ions are in the +5 state, and the Si ions are in the +4 oxidation state. These oxidation-state assignments are also consistent with the coordination geometries of metal ions.

Compound 1

Single-crystal X-ray diffraction analysis shows that the asymmetric unit of **1** consists of one $[PW_{12}O_{40}]^{3-}$ anion and three bpp cations. The central P atom in the disordered "α-Keggin" cluster is tetrahedrally coordinated to four O atoms, and in two crystallographically disordered orientations in a 1:1 ratio. There are alternating "short" and "long" W–O_b–W bonds owing to a small displacement of the W ions from the mirror planes associated with the W_3O_{13} triplets.

There are extensive and effective intermolecular hydrogen bonds among and between the organic cations and inorganic anions. In **1** there are two kinds of distinct supramolecular chains, namely, chains formed from organic bpp ligands and an inorganic-organic hybrid chain (Figure 2). The former is built from bpp (GG′) cations linked through N(1)–H···N(2)^{i} (2.768 Å; i = *x*, –*y*, –1/2 + *z*) hydrogen bonds; the latter is constructed from bpp (TT) cations and Keggin-type anions. The N···O distances are 3.033–3.124 Å, indicating the presence of weak multipoint hydrogen-bond interactions. Thus, an interesting organic bicapped Keggin structure is formed, which is similar to structures that have been reported recently.[17] As shown in Figure 3, the organic and hybrid chains are interlinked to fabricate the 3D supramolecular structure of **1**.

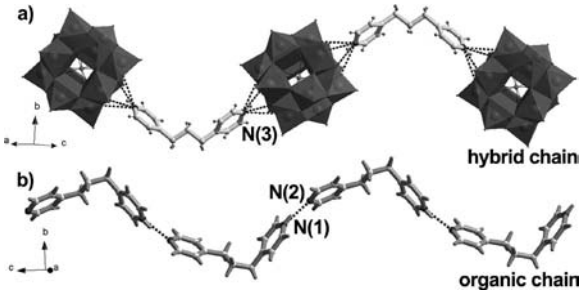

Figure 2. Representations showing the supramolecular chains involving intermolecular hydrogen-bond interactions in **1**: (a) hybrid chain containing organic bicapped Keggin units; (b) chain formed from organic ligand molecules.

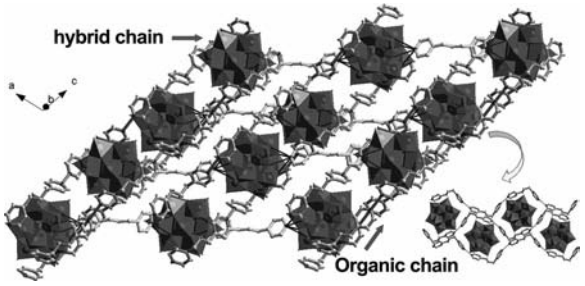

Figure 3. Diagram showing the self-assembly of the organic and hybrid chains in **1**.

Compound 2

Single-crystal X-ray analysis reveals that compound **2** consists of a two-dimensional wavy architecture built from Keggin-type $[SiW_{12}O_{40}]^{4-}$ units linked by Cu^{I}–bpp units (see Figure 4). The Si–O bond within the central tetrahedra of the clusters have lengths within the range of 1.623(8)–1.645(8) Å, and the O–Si–O angles are within the 108.8(4)–110.2(5)° range, indicating that the SiO_4 tetrahedra within this coordination polymer are slightly distorted. The anion has a Keggin structure bisupported by Cu–O bonds [Cu(4)–O(31) 2.561(9), Cu(3)–O(18) 2.562(1) Å; the sum of the van der Waals radii of Cu and O is 2.92 Å[18]].

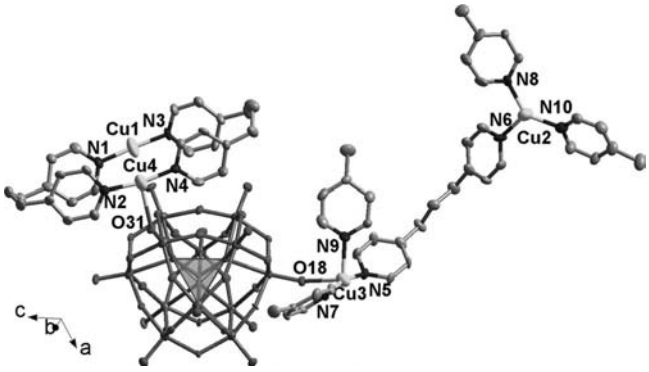

Figure 4. ORTEP drawing showing the linkage units and coordination environment of the Cu centers in **2**. The thermal ellipsoids are drawn at the 30% probability level.

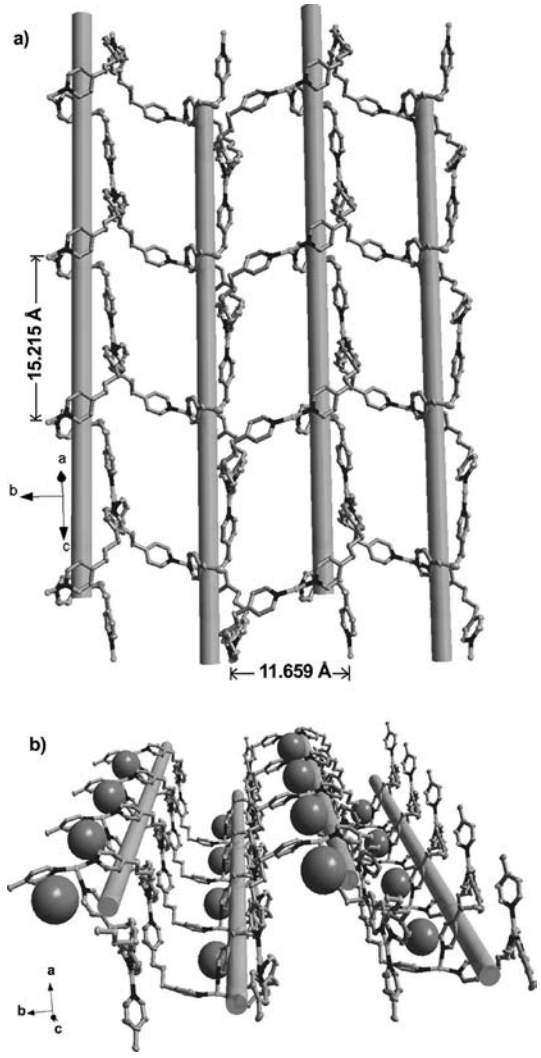

Figure 5. (a) Large porous 2D wavy cationic framework of **2** consisting of $Cu_6(bpp)_6$ grids. $\{[Cu_2(bpp)_2][SiW_{12}O_{40}]\}^{2-}$ fragments are omitted for clarity; (b) chiral monohelical chains with 2_1 symmetry formed by the coordination bonds between Cu^{I} sites and bpp ligands. Spheres: $\{[Cu_2(bpp)_2][SiW_{12}O_{40}]\}^{2-}$ fragments.

Worthy of mention is that there are four crystallographically independent Cu^{I} centers in **2**, and each has a different coordination environment: two-coordinate Cu(1), three-coordinate Cu(2) and Cu(4), and four-coordinate Cu(3). The linear coordinated Cu(1) and T-shaped coordinated Cu(4) share two bent bpp ligands (GG), with Cu–N bond lengths within the 1.880(14)–1.897(14) Å range, resulting in an interesting ring-shaped $Cu_2(bpp)_2$ subunit. Ion Cu(2) is triangularly coordinated by three nitrogen atoms from three bpp ligands with Cu–N distances of 1.964(14), 1.976(18) and 2.032(16) Å, and N–Cu–N angles of 133.2(7) [N(8)–Cu(2)–N(10)], 108.6(6) [N(8)–Cu(2)–N(6)], and 118.2(7)° [N(10)–Cu(2)–N(6)]. Ion Cu(3) has an irregular coordination geometry and is bound to three nitrogen atoms from three bpp with Cu–N distances within the 1.930(13)–2.219(13) Å range, and one oxygen atom from a polyanion [Cu(3)–O(18) 2.562(1) Å].

The assembly of chiral structures from achiral components is of current interest in both coordination chemistry and materials science.[19] The design and construction of chiral frameworks that take advantage of the high symmetry of POM building blocks represents a considerable synthetic challenge.[20] Single-crystal structure analysis indicated that **2** crystallizes in the space group $P2_1$. As shown in Figure 5, compound **2** exhibits an infinite helical layer with 2_1 symmetry, which is created through the formation of coordination bonds between the Cu^{I} sites and bpp ligands. The helical pitch is given by one full rotation around the 2_1 helical axes and is 15.215 Å, this corresponds to the length of the crystallographic *c* axis. The bpp ligands situated between adjacent helical chains connect them together to form a two-dimensional wavy network for which the helical pitch along the *b* axis is 11.656 Å. The chiralities of the metal centers could be extended to the 2D framework consisting of $\{Cu_6(bpp)_6\}$ grids in which $\{[Cu_2(bpp)_2][SiW_{12}O_{40}]\}^{2-}$ fragments are accommodated (see Figure S3, Supporting Information). It might also be supposed that the Keggin-type ions (size ca. 10.5 Å) have a directing role in the structure assembly and ensure that hybrid cationic nets are aggregated, leading to the large porous 2D wavy cationic framework (15.2×11.6 Å^2) observed in **2**.

As shown in Figure 6, the two-dimensional layers are further interconnected through multiform π···π and C–H···O intermolecular interactions to form a three-dimensional supramolecular network. These arrangements reflect not only the flexible geometry of the bpp ligand, but also the coordination preferences of the Cu^{I} sites that adopt linear and T-shaped coordination geometries.

Compound 3

The structural unit of **3** is constructed from one nonclassical Dawson-like polyoxoanion $[H_2SbW_{18}O_{60}]^{7-}$, two $[Cu(Hbpp)_2]^{3+}$ units, half an H_2bpp cation, and three lattice water molecules (Figure 7). The analogous Dawson-like anion $[H_2SbW_{18}O_{60}]^{7-}$ was originally presented by Krebs and Klein,[21] but a complete study of the crystal structure had not been reported. The polyoxoanion $[SbW_{18}O_{60}]^{9-}$ is an antimony-containing Dawson-like polytoxotungstate with approximate D_{3h} point symmetry and contains two B-α-$[Sb_{0.5}W_9O_{33}]^{12.5-}$ moieties linked together through a corner-sharing connection formed by the elimination of six oxygen atoms. Here, the presence of a lone electron pair on the central Sb^{3+} heteroatom, which has a large ionic radius, prevents the formation of a classical Dawson-type cluster, and instead the $[SbW_{18}O_{60}]^{9-}$ anion is preferentially adopted. One {Sb} group is distributed over two central positions of two $\{W_9\}$ entities with fractional occupancies of 0.5 (Sb···Sb 2.167 Å). The Sb^{3+} ion has a pyramidal coordination sphere and is bound to three oxygen atoms, with a lone pair of orbital electrons located at the apex of the pyramid.

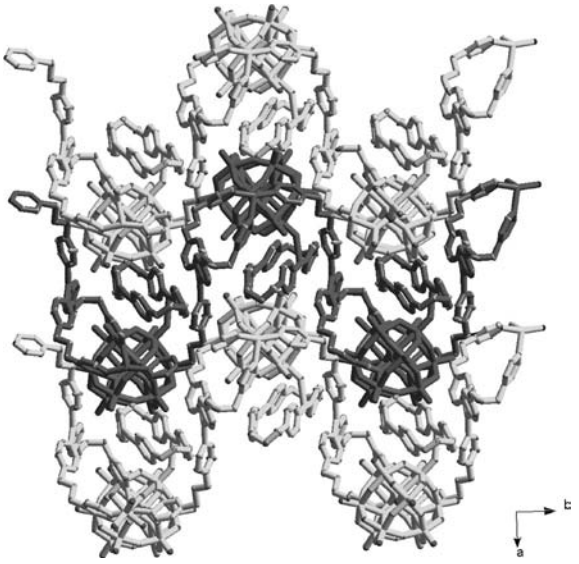

Figure 6. Three-dimensional supramolecular arrangement in **2** that is formed through intermolecular interactions among the 2D wavy layers.

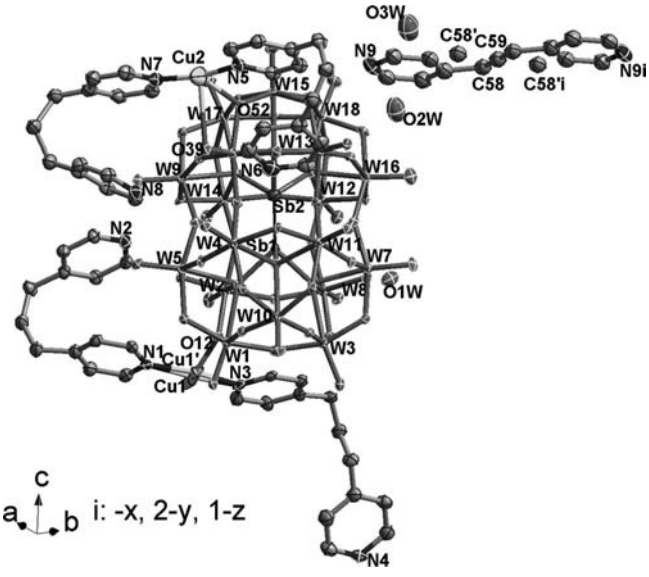

Figure 7. ORTEP drawing of **3** showing the atom labels. The thermal ellipsoids are drawn at the 30% probability level.

The $[SbW_{18}O_{60}]^{9-}$ anion anchors two $[Cu(Hbpp)_2]^{3+}$ groups together with the following bond lengths: Cu(1)–O(12) 2.342(12), Cu(2)–O(52) 2.736(16) Å. Three monoprotonated bpp ligands, guided by directional N–H···O interactions, exhibit GG geometry, thus further demonstrating this ligand's coordination flexibility (see Figure S4, Supporting Information). Both crystallographically independent copper(I) centers adopt T-shaped coordination geometries and are bonded to two nitrogen atoms and one oxygen atom. It should also be noted that Cu(2) is four-coordinate if the weak Cu(2)–O(39) [2.759(19) Å] interaction is taken into account.

Figure 8 clearly shows the intermolecular hydrogen bonds (N–H···O–W and C–H···O–W) that occurred between the inorganic anions and organic cations in **3**. Distances associated with the weak N–H···O–W and C–H···O–W interactions are given in Table S2 (Supporting Information). The crystal packing of compound **3** also illustrates that the polyanions play a directing role in the self-assembly of the organic cations by the involvement of the anion's surface oxygen atoms in the formation of directional hydrogen bonds (see Figure S5, Supporting Information).

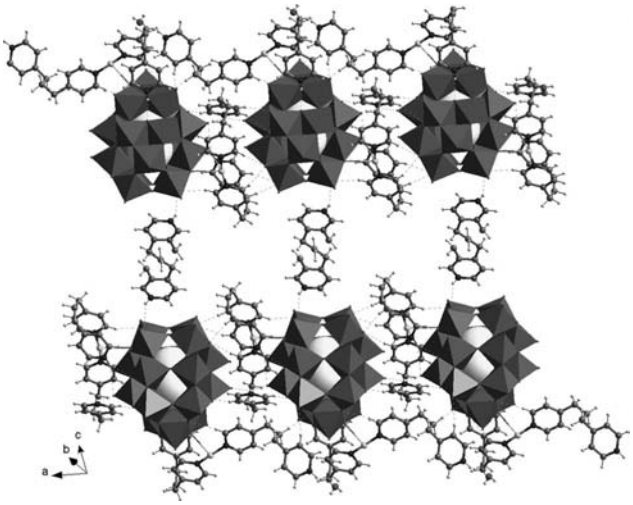

Figure 8. Intermolecular hydrogen-bond interactions that occur among bpp cations and $\{SbW_{18}\}$ clusters in **3**. Polyhedra: $\{WO_6\}$; spheres: Sb ions.

Compound 4

The composition of **4** consists of sandwich-type $[Ni_4(H_2O)_2(AsW_9O_{34})_2]^{10-}$ anions and bpp cations (see Figure 9). The polyoxoanion $[Ni_4(OH_2)_2(AsW_9O_{34})_2]^{10-}$ may be seen as two trilacunary $[B\text{-}\alpha\text{-}(AsW_9O_{34})_2]^{9-}$ fragments from Keggin units joined to four edge-linked $\{NiO_6\}$ octahedra with coplanar nickel ions, leading to a sandwich-type structure with idealized C_{2v} symmetry. The $[B\text{-}\alpha\text{-}(AsW_9O_{34})_2]^{9-}$ units come from saturated Keggin units $[AsW_{12}O_{40}]^{3-}$ from which three adjacent edge-sharing $\{WO_6\}$ octahedra have been removed. There are four crystallographically unique Ni^{II} ions in compound **4**. All of the Ni^{II} centers are octahedrally coordinated with Ni–O distances in the range of 1.95(5)–2.20(5) Å. However, the coordination environments for ions are different: Ni(2) and Ni(4) are coordinated to six oxygen atoms from two different $[B\text{-}\alpha\text{-}(AsW_9O_{34})_2]^{9-}$ units; Ni(1) and Ni(3) are coordinated to five oxygen atoms belonging to two different $[B\text{-}\alpha\text{-}(AsW_9O_{34})_2]^{9-}$ units and one water molecule. The central four $\{NiO_6\}$ octahedra, for which the Ni^{II} ions are coplanar, form a rhombic $\{Ni_4O_{16}\}$ unit. The distances within this unit are: Ni(1)···Ni(2) 3.159, Ni(2)···Ni(3) 3.193, Ni(3)···Ni(4) 3.178, Ni(1)···Ni(4) 3.186, Ni(2)···Ni(4) 3.289, Ni(1)···Ni(3) 5.441 Å; and the angles are Ni(1)···Ni(2)···Ni(3) 117.85, Ni(2)···Ni(3)···Ni(4) 62.17°. These values for the metal–metal separations and the geometry of the bridging unit are very similar to the first example of a sandwich-type phosphorus-containing polyanion, $[Co_4(OH_2)_2\text{-}(PW_9O_{34})_2]^{10-}$, which was reported by Weakley et al.[22]

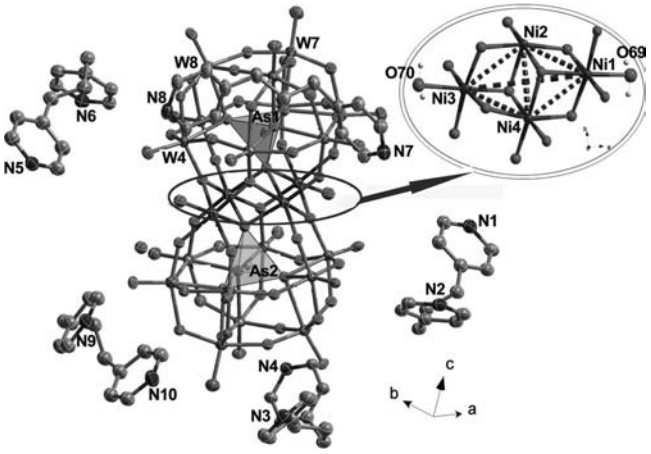

Figure 9. ORTEP drawing of **4** showing the atom labels. The thermal ellipsoids are drawn at the 30% probability level. Polyhedra: $\{AsO_4\}$.

In **4**, the five kinds of crystallographically distinct bpp cations can be grouped into three configurations: two TT, two TG, and one GG. Some typical torsion angles within the bpp cations with TG configuration are: C(12)–C(11)···C(3)–C(2) 106.844, C(11)–C(3)···C(2)–C(1) 37.534°; for cations with TT configuration: C(46)–C(45)···C(40)–C(41) –98.161, C(45)–C(40)···C(41)–C(42) 175.303°; for cations with GG configuration: C(59)–C(58)···C(53)–C(54) 63.358, C(58)–C(53)···C(54)–C(55) –158.753°. Similar to that seen in **1**, four bpp cations cap the surface of one anion to give an interesting tetracapped structure (see Figure S6, Supporting Information). There are extensive and effective intermolecular hydrogen bonds among and between the organic cations and inorganic anions in **4** (see Figure 10 and Figure S7 in the Supporting Information). Some typical intermolecular distances are listed in Table S2 (Supporting Information).

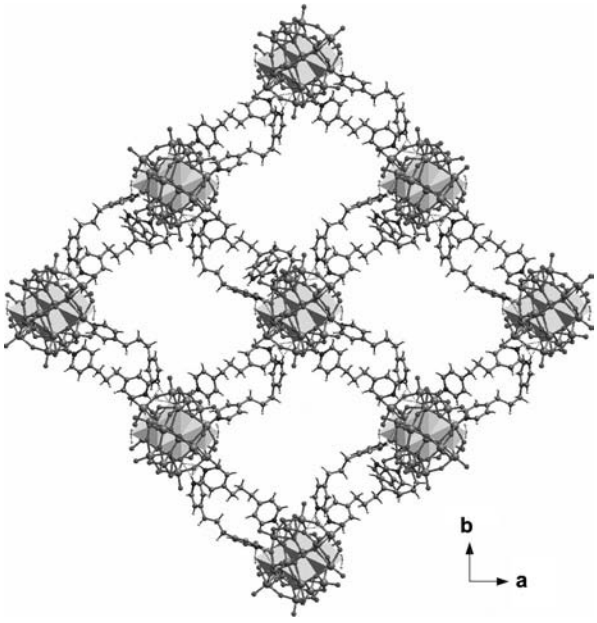

Figure 10. Ball-and-stick view of **4** showing the intermolecular interactions between the sandwich anions and the bpp cations. Polyhedra: {NiO_6}.

Voltammetric Behaviour

The redox properties of **1**–**4** incorporated into carbon paste electrodes (CPE) were studied with the electrodes submerged in 1 M H_2SO_4 aqueous solution. Data were recorded at different scan rates and are shown in Figure S8 (Supporting Information). For **1**-CPE, there are three pairs of reversible redox peaks in the range from 1200 to –900 mV that are ascribed to W: $E_{1/2} = (E_{pa} + E_{pc})/2$ values are –475 mV (I), –93 mV (II), 401 mV (III), and the $\Delta E_p = E_{pa} - E_{pc}$ values are –317 mV (I), 482 mV (II), 745 mV (III) (scan rate: 150 mV s^{-1}). For **2**-CPE, the $E_{1/2} = (E_{pa} + E_{pc})/2$ values are –671 mV (I), –494 mV (II), –13.25 mV (III), and the ΔE_p values are 82 mV (I), 52 mV (II), –184.5 mV (III) (scan rate: 120 mV s^{-1}). For **3**-CPE, the $E_{1/2}$ values for W are –434 mV (I), –340 mV (II), –196 mV (III), and the ΔE_p values are 51 mV (I), 53.5 mV (II), 56.8 mV (III) (scan rate: 80 mV s^{-1}). For **4**-CPE, the $E_{1/2}$ values for W are –640 mV (I), –483 mV (II), 409 mV (III) (scan rate: 100 mV s^{-1}).

When the scan rates were increased, the cathodic peak currents were almost the same as the corresponding anodic ones. Furthermore, the increase in peak-to-peak separation may be explained as follows: (i) the reduction of compounds immobilized in the CPEs is accompanied by the evolution of protons from the solution to maintain charge neutrality. The encapsulation of **1**–**4** into CPEs may slow down the penetration rate of the protons from solution into the particles, and this decreases the electron exchange rate to some extent. With increasing scan rate, the diffusion rate of the protons into the particles begins to determine the rate of electrochemical reduction; (ii) the electron exchange rate between the insoluble solids **1**–**4** and the electrode may be slower than between soluble POM anions and the electrode. CPEs containing compounds **1**–**4** show higher stability than conventional POM gel film electrodes. The electrodes were stable over 100 cycles at a scan rate 80 mV s^{-1}, and the current response remained almost unchanged. The remarkable stability of CPEs containing **1**–**4** can be ascribed to the insolubility of the inorganic-organic hybrid POM particles.

Thermogravimetric Analysis

Thermogravimetric (TG) measurements of **1**–**4** were performed and supported the chemical compositions reported herein (see Figure S9, Supporting Information). Compounds **1** and **2** both comprise bpp cations and Keggin-type clusters. The TG curve for **1** shows a three-step continuous weight loss: the first step is slight, starts at 40 °C, ends at 120 °C, and indicates the removal of water molecules adsorbed on the surface of the crystals. The TG also shows two distinct weight losses that start at 310 °C and end at 820 °C. It should also be noted that the high end temperature for the weight loss is remarkable for this class of structures that are held together through weak interactions. The complete weight loss over this temperature range was 17.21%, corresponds to the decomposition and loss of all the bpp cations from **1**, and is in good agreement with the calculated value of 17.26%. The TG curve for **2** shows that the compound is stable below 280 °C, and above this temperature there is a continuous three-step weight loss event that occurs over the temperature range of 280–730 °C. The complete weight loss at this stage (23.76%) is associated with the removal of bpp and is in good agreement with the calculated value of 24.09%. The TG curves for **3** and **4** also show continuous three-stage weight losses in the 40–800 °C temperature range. The complete weight losses (16.64% for **3** and 23.94% for **4**) correspond to the decomposition and loss of all bpp cations from the structures and are consistent with the calculated values (17.28% for **3** and 23.1% for **4**). All four bpp-based assemblies demonstrated similar stabilities and thermal behaviors despite the different types of anions present in their structures.

Conclusions

Four compounds have been synthesized with the organic ligand bpp that influence the assembly of different polytungstate clusters: α-Keggin clusters in **1** and **2**, a pseudo-Dawson cluster in **3**, and a sandwich-type heteropolyoxoanion in **4**. Compound **1** exhibits an interesting organic bicapped Keggin structure, whereas compound **4** presents a tetracapped sandwich structure. The presence of the Cu-bpp SMG in compound **2** enables it to exhibit a 2D grid-like network that accommodates Keggin anions. However, compound **3** consists only of bisupported $[SbW_{18}O_{60}]^{9-}$ clusters. The bpp molecule may adopt a flexible geometry and wrap around the spherical POM clusters, thus endowing the four compounds with good thermal stability. This work demonstrates how control of the molecular assembly processes can be achieved by the use of structure-

directing anionic polyoxometalate clusters, and flexible organic molecules with freely rotatable C–C single bonds. Extensions to this research, which is concerned with the structural chemistry of these systems, may focus on more flexible organic cations than bpp and the replacement of the inorganic anions with other types of POMs. Studies in this respect are expected to reveal synthetic rules associated with the preparation of these classes of materials and enable the exploration of their attractive properties.

Experimental Section

Materials and Physical Measurements: All chemicals purchased were of reagent grade and used without further purification. Elemental analyses were carried out with a Perkin–Elmer 2400 CHN elemental analyzer. FTIR spectra were recorded over the 400–4000 cm^{-1} range with an Alpha Centaurt FTIR spectrophotometer with KBr pellets. Thermogravimetric differential thermal analysis (TG-DTA) measurements were performed with a Perkin–Elmer Pyris Diamond TG/DTA instrument in flowing N_2 with a heating rate of 10 °C min^{-1}. Hydrothermal syntheses were carried out with a 20 mL Teflon-lined autoclave under autogenous pressure. The reaction vessels were filled to approximately 70% of their volume capacity. Cyclic voltammograms (CV) were recorded with a 384B polarographic analyzer. A CHI 660 Electrochemical Workstation connected to a Digital-586 personal computer controlled the electrochemical measurements and data collections. The data were obtained with a conventional three-electrode system: the working electrode was a modified CPE, the reference electrode was an Ag/AgCl (saturated KCl) electrode, the counter electrode was Pt gauze. All potentials were measured and are reported vs. the Ag/AgCl electrode.

Synthesis of $(Hbpp)_3[PW_{12}O_{40}]$ (1): $H_3[PW_{12}O_{40}]\cdot xH_2O$ (1.5 g) and bpp (20 mg, 0.10 mmol) were dissolved in H_2O (18 mL), and the solution was acidified with 4 M HCl to pH ≈ 5. The resultant solution was stirred in air for ca. 20 min and then sealed in a reactor and heated at 170 °C for 5 d. After slow cooling (10 °C h^{-1}) to room temperature, yellow block crystals were obtained; these were washed with distilled water and dried in air. Yield: ca. 40% (based on W). IR: $\tilde{\nu}$ = 513 (w), 808 (s), 896 (m), 952 (s), 1054 (m), 1100 (w), 1419 (w), 1508 (m), 1635 (m), 1683 (m), 3448 (s) cm^{-1}. $C_{39}H_{46}N_6O_{40}PW_{12}$ (3475.98): calcd. C 13.48, H 1.33, N 2.42; found C 13.63, H 1.41, N 2.36.

Synthesis of $[Cu(bpp)]_2[Cu_2(bpp)_3][SiW_{12}O_{40}]$ (2): A reaction mixture of $K_4[\alpha\text{-}SiW_{12}O_{40}]\cdot 17H_2O$ (650 mg, 0.20 mmol), $CuCl_2\cdot 2H_2O$ (40 mg, 0.24 mmol), and bpp (20 mg, 0.10 mmol) was dissolved in HAc/NaAc buffer solution (15 mL, pH = 4.75). The resultant solution was stirred in air for ca. 2 h and then sealed in a reactor and heated at 180 °C for 5 d. After slow cooling (10 °C h^{-1}) to room temperature, yellow block crystals were obtained; these were washed with distilled water and dried in air. Yield: ca. 35% (based on W). IR: $\tilde{\nu}$ = 532 (w), 667 (w), 798 (s), 869 (m), 919 (s), 970 (m), 1026 (m), 1427 (m), 1500 (w), 1614 (m), 3448 (m) cm^{-1}. $C_{65}H_{70}Cu_4N_{10}O_{40}SiW_{12}$ (4119.78): calcd. C 18.94, H 1.71, N 3.40; found C 18.63, H 1.82, N 3.36.

Synthesis of $[Cu_2(Hbpp)_4](H_2bpp)_{0.5}H_2[SbW_{18}O_{60}]\cdot 3H_2O$ (3): A reaction mixture of Sb_2O_3 (60 mg, 0.21 mmol), $CuCl_2\cdot 2H_2O$ (40 mg, 0.24 mmol), $Cu(CH_3COO)_2\cdot H_2O$ (40 mg, 0.20 mmol), bpp (40 mg, 0.20 mmol), $Na_2WO_4\cdot 2H_2O$ (700 mg, 2.12 mmol) and H_2O (15 mL) was adjusted to pH ≈ 3.1 with dilute HCl solution. The resulting solution was sealed in a reactor and heated at 170 °C for 6 d. Light yellow crystals were obtained. Yield: ca. 23% (based on W). IR: $\tilde{\nu}$ = 765 (s), 879 (s), 958 (s), 1126 (w), 1432 (m), 1506 (m), 1618 (s), 2362 (m), 3413 (s) cm^{-1}. $C_{117}H_{152}Cu_4N_{18}O_{126}Sb_2W_{36}$ (10942.48): calcd. C 12.84, H 1.40, N 2.30; found C 12.63, H 1.51, N 2.22.

Synthesis of $(H_2bpp)_5[Ni_4(OH_2)_2(AsW_9O_{34})_2]\cdot 0.5H_2O$ (4): A mixture of $Na_3AsO_4\cdot 12H_2O$ (200 mg, 0.47 mmol), $Na_2WO_4\cdot 2H_2O$ (350 mg, 1.06 mmol), $NiSO_4\cdot 6H_2O$ (40 mg, 0.15 mmol), and bpp (50 mg, 0.25 mmol) was dissolved in distilled water (10 mL) at room temperature and stirred for 3 h. Then the pH value of the mixture was adjusted with 4 mol L^{-1} HCl to ca. 6, and then the mixture was stirred for another 1 h. Finally, the suspension was placed in a Teflon-lined autoclave and kept under autogenous pressure at 150 °C for 10 d. After slow cooling to room temperature, yellow block crystals were removed by filtration and washed with

Table 1. Crystal data and structure refinement details for **1**–**4**.

	1	**2**	**3**	**4**
Empirical formula	$C_{39}H_{46}N_6O_{40}PW_{12}$	$C_{65}H_{70}Cu_4N_{10}O_{40}SiW_{12}$	$C_{117}H_{146}Cu_4N_{18}O_{126}Sb_2W_{36}$	$C_{130}H_{170}As_4N_{20}Ni_8O_{141}W_{36}$
Formula mass	3475.99	4119.76	10936.48	11656.29
Crystal system	monoclinic	monoclinic	triclinic	tetragonal
a [Å]	24.262(4)	14.0574(13)	13.5372(9)	26.427(3)
b [Å]	12.6734(18)	23.305(2)	14.5966(10)	26.427(3)
c [Å]	21.987(3)	15.2152(14)	28.2902(19)	66.560(5)
α [°]	90	90	87.2340(10)	90
β [°]	107.080(2)	115.8590(10)	78.2390(10)	90
γ [°]	90	90	64.0630(10)	90
Unit cell volume [$Å^3$]	6462.5(16)	4485.4(7)	4916.2(6)	46483(8)
Temperature [K]	273(2)	273(2)	296(2)	298(2)
Space group	*C*2/*c*	*P*2(1)	$P\bar{1}$	*I*4(1)*cd*
Z	4	2	1	8
No. of reflections measured	17692	25050	35875	85235
No. of independent reflections	6324	15016	24113	19687
R_{int}	0.0332	0.0372	0.0483	0.1945
Flack parameter		–0.019(9)		0.00(5)
Final R_1 values [$I > 2\sigma(I)$]	0.0419	0.0368	0.0531	0.0987
Final $wR(F^2)$ values [$I > 2\sigma(I)$]	0.0987	0.0821	0.1309	0.2016
Final R_1 values (all data)	0.0527	0.0418	0.0856	0.2131
Final $wR(F^2)$ values (all data)	0.1031	0.0846	0.1707	0.2884
Goodness of fit on F^2	1.070	0.996	1.058	1.091

distilled water. Yield: ca. 39% (based on W). IR: $\tilde{\nu}$ = 763 (m), 883 (s), 952 (m), 1400 (s), 1508 (m), 1635 (s), 2360 (m), 3100 (m), 3401 (s) cm^{-1}. $C_{130}H_{169}As_4N_{20}Ni_8O_{141}W_{36}$ (11655.29): calcd. C 13.40, H 1.46, N 2.40; found C 13.27, H 1.48, N 2.36.

X-ray Crystallography: Data for compounds **1**–**4** were collected at room temperature with a Bruker Smart Apex CCD diffractometer and with Mo-K_α monochromated radiation (λ = 0.71703 Å). Routine Lorentz and polarization corrections were applied to the data. The structures of **1**–**4** were solved by direct methods and refined by the full-matrix least-squares methods on F^2 with the SHELXTL crystallographic software package.[23] Anisotropic thermal parameters were refined for all non-hydrogen atoms. The positions of the hydrogen atoms attached to carbon atoms were fixed at ideal positions. Hydrogen atoms attached to nitrogen atoms were located from the difference Fourier maps and were constrained. A summary of the crystallographic data and structural determination parameters for **1**–**4** are provided in Table 1. Details of the intermolecular hydrogen-bond interactions in the crystal structures of **1**–**4** are provided in Table S2 (Supporting Information). Some typical bond lengths in **1**–**4** are given in Table S3 (Supporting Information). CCDC-779862 (for **1**), -779863 (for **2**), -779864 (for **3**), -779865 (for **4**) contain the supplementary crystallographic data for this paper. These data can be obtained free of charge from The Cambridge Crystallographic Data Centre via www.ccdc.cam.ac.uk/data_request/cif.

Preparation of Modified Carbon Paste Electrodes Containing Compounds 1–4: Graphite powder (0.5 g) and the relevant compound (0.05 g) were mixed and ground together with an agate mortar and pestle to achieve a uniform and dry mixture. Paraffin oil (0.5 mL) was added to the mixture, while it was stirred with a glass rod. Then the mixture was packed into a glass tube (3 mm inner diameter), and the surface of the mixture was pressed firmly onto weighing paper with a copper rod inserted at the other end of the tube. An electrical contact was established with a copper rod situated on the back of the electrode.

Supporting Information (see footnote on the first page of this article): XRD, IR, TG, electrochemical analysis curves, other figures and crystal data for **1**–**4**, typical bond lengths and details of intermolecular hydrogen bond interactions for **1**–**4**.

Acknowledgments

This work was financially supported by the National Natural Science Foundation of China (20701011, 20731002 and 20671011), the China Postdoctoral Science Foundation (20070410037, and 20801045), the Natural Science Foundation of Hebei Province (No. B2011205035), and the Education Department Foundation of Hebei Province (Z2006436).

[1] a) H. N. Miras, G. J. T. Cooper, D. L. Long, H. Bögge, A. Müller, C. Streb, L. Cronin, *Science* **2010**, *327*, 72–74; b) P. P. Mishra, J. Pigga, T. B. Liu, *J. Am. Chem. Soc.* **2008**, *130*, 1548–1549; c) Q. S. Yin, J. M. Tan, C. Besson, Y. V. Geletii, D. G. Musaev, A. E. Kuznetsov, Z. Luo, K. I. Hardcastle, C. L. Hill, *Science* **2010**, *328*, 342–345.

[2] a) R. Tsunashima, D. L. Long, H. N. Miras, D. Gabb, C. P. Pradeep, L. Cronin, *Angew. Chem.* **2010**, *122*, 117–120; *Angew. Chem. Int. Ed.* **2010**, *49*, 113–116; b) C. P. Pradeep, D. L. Long, G. N. Newton, Y. F. Song, L. Cronin, *Angew. Chem.* **2008**, *120*, 4460–4463; *Angew. Chem. Int. Ed.* **2008**, *47*, 4388–4391; c) A. M. Khenkin, R. Neumann, *J. Am. Chem. Soc.* **2008**, *130*, 14474–14476; d) G. G. Gao, P. S. Cheng, T. C. W. Mak, *J. Am. Chem. Soc.* **2009**, *131*, 18257–18259; e) B. Botar, P. Kögerler, C. L. Hill, *Inorg. Chem.* **2007**, *46*, 5398–5403.

[3] a) Y. Ishii, Y. Takenaka, K. Konishi, *Angew. Chem.* **2004**, *116*, 2756–2759; *Angew. Chem. Int. Ed.* **2004**, *43*, 2702–2705; b) J. M. Knaust, C. Inman, S. W. Keller, *Chem. Commun.* **2004**, 492–493; c) Z. H. Peng, *Angew. Chem.* **2004**, *116*, 948–953; *Angew. Chem. Int. Ed.* **2004**, *43*, 930–935; d) J. Y. Niu, P. T. Ma, H. Y. Niu, J. Li, J. W. Zhao, Y. Song, J. P. Wang, *Chem. Eur. J.* **2007**, *13*, 8739–8748; e) J. W. Zhao, H. P. Jia, J. Zhang, S. T. Zheng, G. Y. Yang, *Chem. Eur. J.* **2007**, *13*, 10030–10045; f) S. T. Zheng, J. Zhang, G. Y. Yang, *Angew. Chem.* **2008**, *120*, 3973–3977; *Angew. Chem. Int. Ed.* **2008**, *47*, 3909–3913.

[4] a) J. Q. Sha, J. Peng, H. S. Liu, J. Chen, A. X. Tian, P. P. Zhang, *Inorg. Chem.* **2007**, *46*, 11183–11189; b) X. B. Cui, J. Q. Xu, Y. Li, Y. H. Sun, G. Y. Yang, *Eur. J. Inorg. Chem.* **2004**, *5*, 1051–1055; c) X. L. Wang, C. Qin, E. B. Wang, Z. M. Su, Y. G. Li, L. Xu, *Angew. Chem.* **2006**, *118*, 7571–7574; *Angew. Chem. Int. Ed.* **2006**, *45*, 7411–7414.

[5] a) H. Y. An, E. B. Wang, D. R. Xiao, Y. G. Li, Z. M. Su, L. Xu, *Angew. Chem.* **2006**, *118*, 918–922; *Angew. Chem. Int. Ed.* **2006**, *45*, 904–908; b) Y. Xu, L. H. An, L. L. Koh, *Chem. Mater.* **1996**, *8*, 814–818; c) X. L. Wang, Y. F. Bi, B. K. Chen, H. Y. Lin, G. C. Liu, *Inorg. Chem.* **2008**, *47*, 2442–2448; d) Y. P. Ren, X. J. Kong, L. S. Long, R. B. Huang, L. S. Zheng, *Cryst. Growth Des.* **2006**, *6*, 572–576.

[6] Y. F. Song, D. L. Long, L. Cronin, *Angew. Chem.* **2007**, *119*, 3974–3978; *Angew. Chem. Int. Ed.* **2007**, *46*, 3900–3904.

[7] a) E. Coronado, J. R. Galán-Mascarós, C. Giménez-Saiz, C. J. Gómez-García, E. Martínez-Ferrero, M. Almeida, E. B. Lopes, S. C. Capelli, R. M. Llusar, *J. Mater. Chem.* **2004**, *14*, 1867–1872; b) E. Coronado, C. Giménez-Saiz, C. J. Gómez-García, S. C. Capelli, *Angew. Chem.* **2004**, *116*, 3084–3087; *Angew. Chem. Int. Ed.* **2004**, *43*, 3022–3025.

[8] a) D. L. Long, E. Burkholder, L. Cronin, *Chem. Soc. Rev.* **2007**, *36*, 105–121; b) T. B. Liu, E. Diemann, H. L. Li, A. W. M. Dress, A. Müller, *Nature* **2003**, *426*, 59–61.

[9] a) D. L. Long, L. Cronin, *Chem. Eur. J.* **2006**, *12*, 3698–3706; b) Y. F. Song, N. McMillan, D. L. Long, J. Thiel, Y. L. Ding, H. S. Chen, N. Gadegaard, L. Cronin, *Chem. Eur. J.* **2008**, *14*, 2349–2354.

[10] C. P. Pradeep, D. L. Long, G. N. Newton, Y. F. Song, L. Cronin, *Angew. Chem.* **2008**, *120*, 4460–4463; *Angew. Chem. Int. Ed.* **2008**, *47*, 4388–4391.

[11] a) Z. G. Han, Y. L. Zhao, J. Peng, H. Y. Ma, Q. Liu, E. B. Wang, N. H. Hu, H. Q. Jia, *Eur. J. Inorg. Chem.* **2005**, *2*, 264–271; b) Z. G. Han, Y. L. Zhao, J. Peng, A. X. Tian, Q. Liu, J. F. Ma, E. B. Wang, N. H. Hu, *CrystEngComm* **2005**, *7*, 380–387; c) Z. G. Han, Y. L. Zhao, J. Peng, Q. Liu, E. B. Wang, *Electrochim. Acta* **2005**, *51*, 218–224; d) A. X. Tian, J. Ying, J. Peng, J. Q. Sha, Z. G. Han, J. F. Ma, Z. M. Su, N. H. Hu, H. Q. Jia, *Inorg. Chem.* **2008**, *47*, 3274–3283.

[12] a) Z. G. Han, Y. L. Zhao, J. Peng, A. X. Tian, Y. H. Feng, Q. Liu, *J. Solid State Chem.* **2005**, *178*, 1386–1394; b) Z. G. Han, Y. L. Zhao, J. Peng, H. Y. Ma, Q. Liu, E. B. Wang, N. H. Hu, *J. Solid State Chem.* **2004**, *177*, 4325–4331; c) Z. G. Han, Y. L. Zhao, J. Peng, H. Y. Ma, Q. Liu, E. B. Wang, *J. Mol. Struct.* **2005**, *738*, 1–7; d) A. X. Tian, Z. G. Han, J. Peng, J. L. Zhai, Y. L. Zhao, *Z. Anorg. Allg. Chem.* **2007**, *633*, 495–503.

[13] a) Z. G. Han, Y. G. Gao, C. W. Hu, *Cryst. Growth Des.* **2008**, *8*, 1261–1264; b) Z. G. Han, Y. G. Gao, X. L. Zhai, J. Peng, A. X. Tian, Y. L. Zhao, C. W. Hu, *Cryst. Growth Des.* **2009**, *9*, 1225–1234.

[14] a) L. Carlucci, G. Ciani, D. M. Proserpio, S. Rizzato, *CrystEngComm* **2002**, *4*, 121–129; b) S. C. Manna, A. D. Jana, G. M. Rosair, M. G. B. Drew, G. Mostafa, N. R. Chaudhuri, *J. Solid State Chem.* **2008**, *181*, 457–466.

[15] a) C. D. Wu, C. Z. Lu, H. H. Zhuang, J. S. Huang, *Inorg. Chem.* **2002**, *41*, 5636–5637; b) C. M. Liu, D. Q. Zhang, D. B. Zhu, *Cryst. Growth Des.* **2005**, *5*, 1639–1642; c) Y. P. Ren, X. J. Kong, X. Y. Hu, M. Sun, L. S. Long, R. B. Huang, L. S.

Zheng, *Inorg. Chem.* **2006**, *45*, 4016–4023; d) K. Pavani, S. E. Lofland, K. V. Ramanujachary, A. Ramanan, *Eur. J. Inorg. Chem.* **2007**, 568–578; e) Y. Q. Lan, S. L. Li, X. L. Wang, K. Z. Shao, D. Y. Du, H. Y. Zang, Z. M. Su, *Inorg. Chem.* **2008**, *47*, 8179–8187; f) Z. G. Han, T. Chai, X. L. Zhai, J. Y. Wang, C. W. Hu, *Solid State Sci.* **2009**, *11*, 1998–2002.

[16] I. D. Brown, D. Alternatt, *Acta Crystallogr., Sect. B* **1985**, *41*, 244–247.

[17] Z. G. Han, T. Chai, Y. N. Wang, Y. Z. Gao, C. W. Hu, *Polyhedron* **2010**, *29*, 196–203.

[18] A. Bondi, *J. Phys. Chem.* **1964**, *68*, 441–452.

[19] a) C. Piguet, G. Dernardinelli, G. Hopfgartner, *Chem. Rev.* **1997**, *97*, 2005–2062; b) C. He, Y. G. Zhao, D. Guo, Z. H. Lin, C. Y. Duan, *Eur. J. Inorg. Chem.* **2007**, *22*, 3451–3463.

[20] D. B. Dang, H. Gao, Y. Bai, X. F. Hu, F. Yang, Y. Chen, J. Y. Niu, *Inorg. Chem. Commun.* **2010**, *13*, 37–41.

[21] B. Krebs, R. Klein in *Polyoxometalates: From Platonic Solids to Anti-Retroviral Activity* (Eds.: M. T. Pope, A. Müller), Kluwer Academic Publishers, Dordrecht, **1994**, pp. 55.

[22] T. J. R. Weakley, H. T. Evans, J. S. Showell, G. F. Tourné, C. M. Tourné, *J. Chem. Soc., Chem. Commun.* **1973**, 139–140.

[23] a) G. M. Sheldrick, *SHELXS-97, Program for Crystal Structure Solution*, University of Göttingen, Göttingen, Germany, **1997**; b) G. M. Sheldrick, *SHELXL-97, Program for Crystal Structure Refinement*, University of Göttingen, Göttingen, Germany, **1997**.

Received: January 16, 2011
Published Online: June 1, 2011

